Biology of Reproduction, 2021, 104(2), 457–467
doi:10.1093/biolre/ioaa198
Research Article
Advance Access Publication Date: 28 October 2020

OXFORD

Research Article

Mesenchymal stromal cell-derived extracellular vesicle therapy prevents preeclamptic physiology through intrauterine immunomodulation†

Elizabeth S. Taglauer[1,2], Angeles Fernandez-Gonzalez[1,2], Gareth R. Willis[1,2], Monica Reis[1,2], Vincent Yeung[1,2], Xianlan Liu[1,2], S. Alex Mitsialis[1,2] and Stella Kourembanas[1,2,*]

[1]Division of Newborn Medicine and Department of Pediatrics, Boston Children's Hospital, Boston, MA, USA and [2]Department of Pediatrics, Harvard Medical School, Boston, MA, USA

*__Correspondence:__ Division of Newborn Medicine and Department of Pediatrics, Boston Children's Hospital, 300 Longwood Ave. Enders 961, Boston, MA 02115, USA. Tel: 617-919-2355; Fax: 617-730-0260; E-mail: stella.kourembanas@childrens.harvard.edu

†__Grant Support:__ This work was supported by National Institutes of Health R01 HL146128, R21 AI134025 (SK); Hood Foundation Major Grants Initiative to Advance Child Health (SK); NIH T32 Integrated Training in Respiratory Research and Newborn Medicine Research (EST); AAP Marshall Klaus Award (EST).

Received 12 June 2020; Revised 29 September 2020; Accepted 23 October 2020

Abstract

Human umbilical cord-derived mesenchymal stromal cells (MSCs) are a widely recognized treatment modality for a variety of preclinical disease models and have been transitioned to human clinical trials. We have previously shown in neonatal lung disease that the therapeutic capacity of MSCs is conferred by their secreted extracellular vesicles (MEx), which function primarily through immunomodulation. We hypothesize that MEx have significant therapeutic potential pertinent to immune-mediated gestational diseases. Of particular interest is early-onset preeclampsia, which can be caused by alterations of the maternal intrauterine immune environment. Using a heme-oxygenase-1 null mouse model of pregnancy loss with preeclampsia-like features, we examined the preventative effects of maternal MEx treatment early in pregnancy. Heme oxygenase-1 null females ($Hmox1^{-/-}$) or wild-type control females were bred in homozygous matings followed by evaluation of maternal and fetal parameters. A single dose of MEx was administered intravenously on gestational day (GD)1 to $Hmox1^{-/-}$ females ($Hmox1^{-/-}$ MEx). Compared with untreated $Hmox1^{-/-}$ females, $Hmox1^{-/-}$ MEx-treated pregnancies showed significant improvement in fetal loss, intrauterine growth restriction, placental spiral artery modification, and maternal preeclamptic stigmata. Biodistribution studies demonstrated that MEx localize to a subset of cells in the preimplantation uterus. Further, mass cytometric (CyTOF) evaluation of utero-placental leukocytes in $Hmox1^{-/-}$ MEx versus untreated pregnancies showed alteration in the abundance, surface marker repertoire, and cytokine profiles of multiple immune populations. Our data demonstrate the therapeutic potential of MEx to optimize the intrauterine immune environment and prevent maternal and fetal sequelae of preeclamptic disease.

Summary sentence

Antenatal administration of human umbilical cord mesenchymal stromal cell-derived extracellular vesicles prevents pregnancy loss, fetal growth restriction, and preeclamptic physiology through multiparameter modulation of intrauterine leukocytes.

Key words: preeclampsia, fetal growth restriction, mesenchymal stromal cells, extracellular vesicles, biologic therapeutics, macrophages, dendritic cells, uterine natural killer cells, immunomodulation.

Introduction

Preeclampsia affects approximately 3–5% of pregnancies worldwide and is the leading cause of fetal growth restriction in non-anomalous infants [1]. A heterogeneous disease with multifactorial pathogenesis, it presents most commonly with unified maternal symptoms of hypertension, renal glomerular disruption with proteinuria, liver dysfunction, and potential for maternal seizures. A subset of early onset, severe preeclamptic pregnancies involve alterations in the uterine immune environment leading to abnormal placentation, fetal growth restriction, and increased risk for pregnancy loss [2–4]. Due to its multifactorial etiology, preeclampsia remains difficult to treat despite a variety of attempted interventions [2]. Existing pharmacologic agents can attenuate certain maternal symptoms, but no clinically available therapies to date have been able to prevent preeclampsia onset and/or mitigate the fetal consequences of this disease. As the source of the most severe immune-mediated preeclamptic disease stems from utero-placental dysregulation, therapies modulating the intrauterine environment will be crucial in improving both maternal and fetal outcomes.

Mesenchymal stromal cells (MSCs) are well characterized for their ability to ameliorate a variety of disease processes [5, 6]. With pluripotent capabilities, these cells are primarily involved in tissue homeostasis. Though MSCs can migrate to injured tissues, they have limited ability for long-term engraftment/expansion. Our group and several others have demonstrated that soluble mediators derived from MSCs can efficaciously convey their therapeutic effects [7–11]. Of particular interests are MSC-derived extracellular vesicles [12, 13] and, in particular, the smaller population (<150 nm in diameter), which includes exosomes, the extracellular vesicles generated via the endocytic pathway [14]. Exosomes contain a variety of surface proteins and cargo including immunomodulatory proteins, cytokines, messenger RNAs, and microRNAs [9]. MSC-derived extracellular vesicles (MEx), harvested from MSC-conditioned media, have potent immunomodulatory capabilities but low immunogenic potential, which makes them a particularly interesting therapy for immune-mediated diseases [15]. There has been increasing awareness of biologic therapeutics for preeclampsia, including the utility of MSC-based treatments [16, 17]. As the pathogenesis of preeclampsia can involve alterations in the intrauterine immune environment [2], we hypothesize that MEx can optimize the intrauterine environment to prevent preeclamptic disease and its sequelae.

To explore this hypothesis, we investigated the heme oxygenase-1 (HO-1, product of the Hmox1 gene) knockout (KO) mouse model of preeclampsia [18]. HO-1 is primarily involved in heme degradation producing carbon monoxide, iron, and biliverdin. As a stress-inducible enzyme, HO-1 is also an important mediator of immune homeostasis particularly in myeloid populations [19]. Alterations in HO-1 expression have been associated with preeclampsia in human pregnancy and the absence of HO-1 in murine gestation has a phenotype of fetal loss/growth restriction with altered placentation and maternal preeclampsia-like features [18, 20, 21]. Similar to humans, the murine preeclampsia-like phenotype of Hmox1$^{-/-}$ pregnancy appears to have a multifactorial etiology, with evidence of systemic maternal vascular changes, alterations in key placental immune populations, and evidence of intrauterine inflammation [22]. Utilizing the Hmox1$^{-/-}$ model system, we tested the therapeutic capacity of MEx to ameliorate pregnancy loss as well as preeclamptic stigmata and investigated its potential to modulate intrauterine immune populations.

Materials and methods

MEx isolation and characterization

MSC and MEx were isolated using a protocol established by our research group (Supplemental Figure S1) [23]. Briefly, MSCs were isolated from term healthy umbilical cord Wharton jelly using a modified in vitro explant culture technique as previously described [7]. Resultant MSCs were then cultured in alpha-modified Eagle medium (plus nucleosides, Invitrogen) supplemented with 10% fetal bovine serum (Invitrogen), 2 mM L-glutamine and 1% penicillin/streptomycin in p150 dishes (Corning) at 37°C in a humidified atmosphere with 5% CO_2 and allowed to reach a confluency of 60–70% prior to each passage.

MSC differentiation potential at passage (P)2 was assessed using differentiation assay kits for chondrogenesis, adipogenesis, and osteogenesis, per manufacturer instructions (StemPro, Gibco). Ability to differentiate into these three lineages was used as early confirmation of MSC morphology for each MEx prep (Supplemental Figure S1A). MSC purity at P2 was further evaluated via single-color flow cytometry (Supplemental Figure S1B) using fluorescently conjugated antibodies against human MSC positive markers CD105, CD90, CD73, and CD44 (BD Pharmingen) as well a human MSC negative marker panel (BD Pharmingen).

For exosome harvest (Supplemental Figure S1A), MSC preps were further cultured to P3, and upon reaching 90% confluency, cells were serum starved for 36 h followed by collection of cell culture supernatant (conditioned media). This conditioned media was then subjected to differential centrifugation and exosome isolation by flotation on an OptiPrep (iodixanol) cushion (Sigma) (Supplemental Figure S1C). Isolated exosomal content in fraction 9 (MEx-enriched fraction) was then confirmed by western blot showing positive expression of exosome-specific surface proteins ALIX, CD63, CD81, and syntenin-1 as well as negative expression of GM130 [23] (Supplemental Figure S1D). Antibodies for western blot analysis were sourced as follows: ALIX (Santa Cruz), CD63 (Sigma-Aldrich), CD81 (Santa Cruz), syntenin-1 (Thermo Fisher), and GM130 (Cell Signaling). Purified MEx were additionally evaluated using NanoSight analysis to assess particle size distribution/concentration (Supplemental Figure S1E) as well as

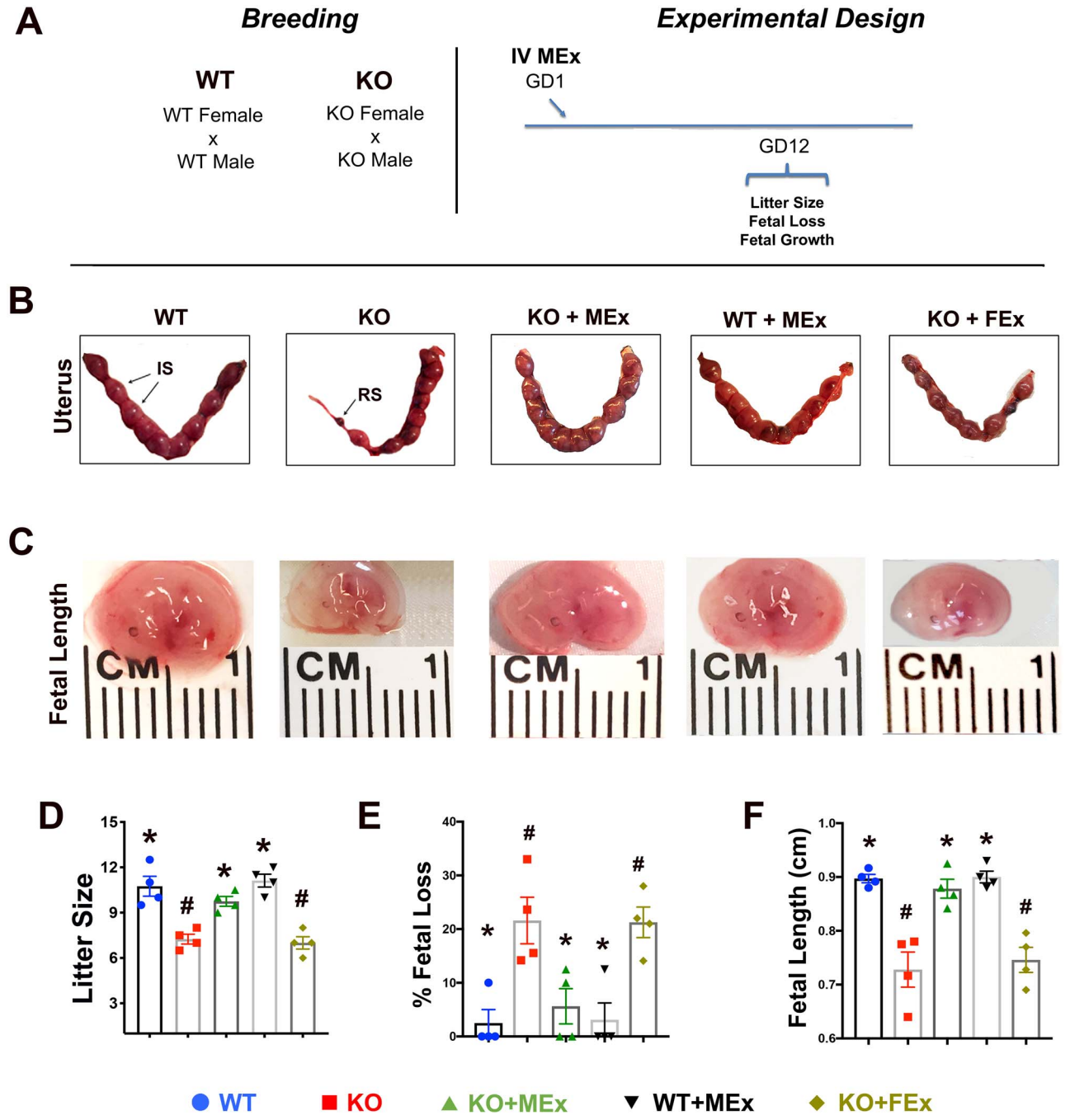

Figure 1. Fetal loss and growth restriction are prevented by MEx treatment. Analysis of uterine and fetal tissues at GD12. (A) Experimental design. (B) H&E histology of renal glomeruli at GD12, Images 100× magnification, scale bars 50um. Black arrows denote areas of eosin-positive proteinaceous material. (C) ELISA analysis of maternal urine albumin at GD12. (D) Maternal tail-cuff blood pressure throughout gestation. All images and graphical analyses representative of three independent experiments, three to four pregnant dams/experiment. Statistical significance ($P < 0.05$), as determined by one-way analysis of variance, denoted by different symbols (*, #, S).

electron microscopy to visualize vesicle morphology and size in each prep (Supplemental Figure S1F).

For control injections, fibroblast-derived extracellular vesicles were generated from human foreskin dermal fibroblast cells as previously described [7].

Timed pregnancies and MEx treatment

The *Hmox1* gene KO mouse colony ($Hmox1^{-/-}$) used for this study was on a mixed Balb/c, 129/sv3 background and generated as previously described [24]. $Hmox1^{-/-}$ mice were generated from $Hmox^{+/-}$ progenitors. Wild-type (WT) littermates utilized for all experiments were also on a Balb/c, 129/sv3 background. Timed pregnancies of WT and $Hmox1^{-/-}$ (KO) mice were conducted by breeding of either homozygous (KO × KO) or hemizygous (KO × WT) pairs with the detection of a vaginal plug as GD0. A single dose of purified MEx (5×10^6 cell equivalents) was then administered via tail vein injection at GD1 (Figure 1). This MEx dose for has been previously established in our lab as capable of

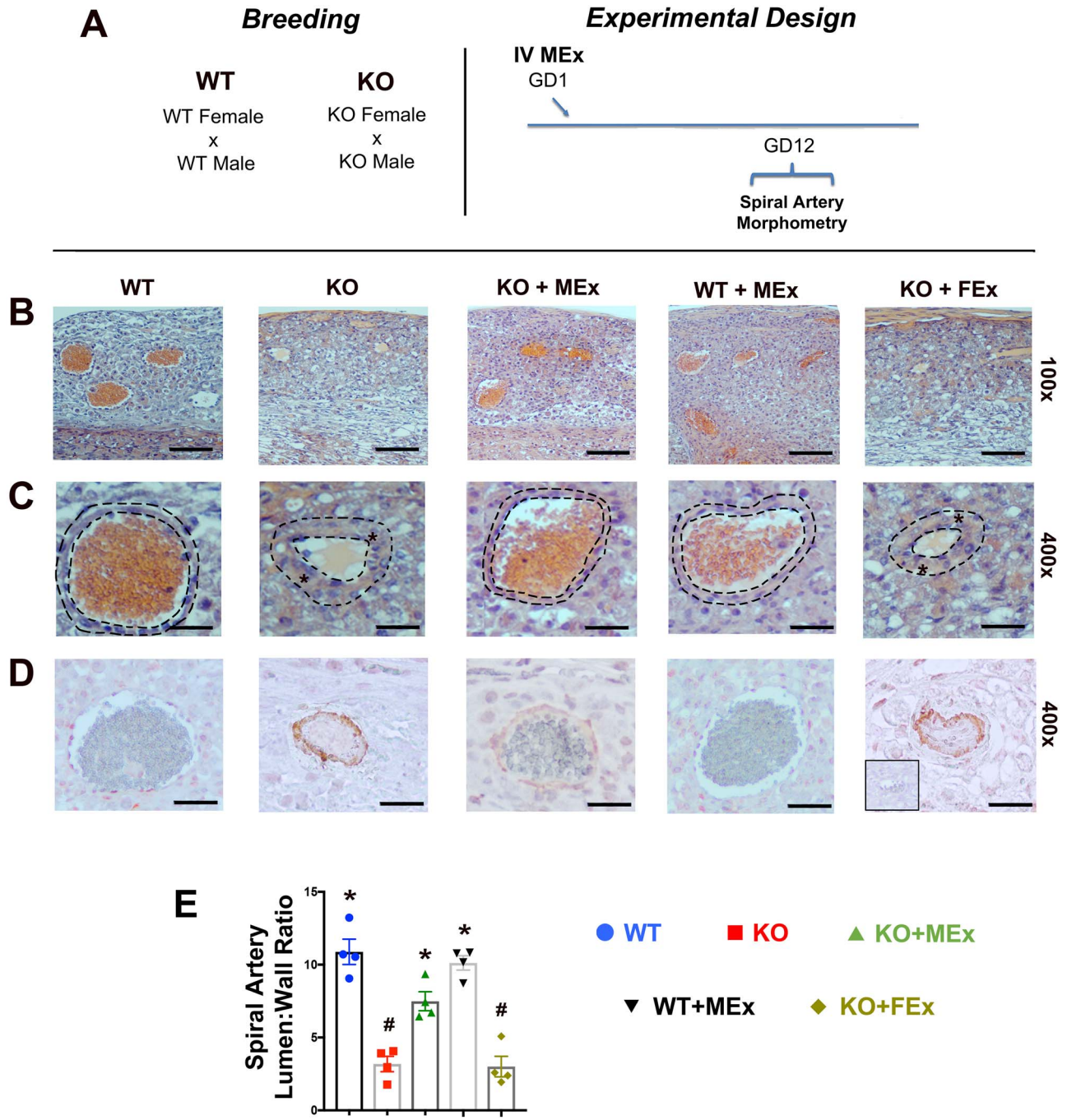

Figure 2. Spiral artery morphology is altered by antenatal MEx treatment. (A) Experimental design. (B, C) Representative H&E images of spiral arteries at (B) low magnification (×100) and (C) high magnification (×400). Dotted lines denote area of analysis for lumen:wall ratios. Stars denote thickened blood vessel walls. (D) Representative images of smooth muscle actin immunohistochemistry. Red stain: smooth muscle actin; blue stain: hematoxylin nuclear stain. Inset black box: second only negative control. (E) Graphical analysis representative of four independent experiments, total $n = 12–16$ placentas for each condition. Scale bars ×100: 50 μm, ×400: 15 μm. Statistical significance ($P < 0.05$) as determined by one-way analysis of variance is denoted by different symbols (*, #).

conferring therapeutic effects in adult murine models of pulmonary hypertension and pulmonary fibrosis [12, 25].

Pregnancy evaluation and tissue collection

On GD12, pregnant female mice were sacrificed via intraperitoneal pentobarbital injection followed by dissection and removal of gravid uteri. Fetal implantation sites (IS) and resorption sites (RS) were enumerated and recorded for evaluation of pregnancy loss. Then using a modified cesarean section technique, intact fetuses were removed from the uterus followed by measurement of fetal crown rump length. From the same uteri, remaining tissues of the IS (including uterus, metrial gland, and placental tissues) were further processed for mass cytometry analysis. Finally, maternal kidneys were harvested and placed into formalin for further histological analysis.

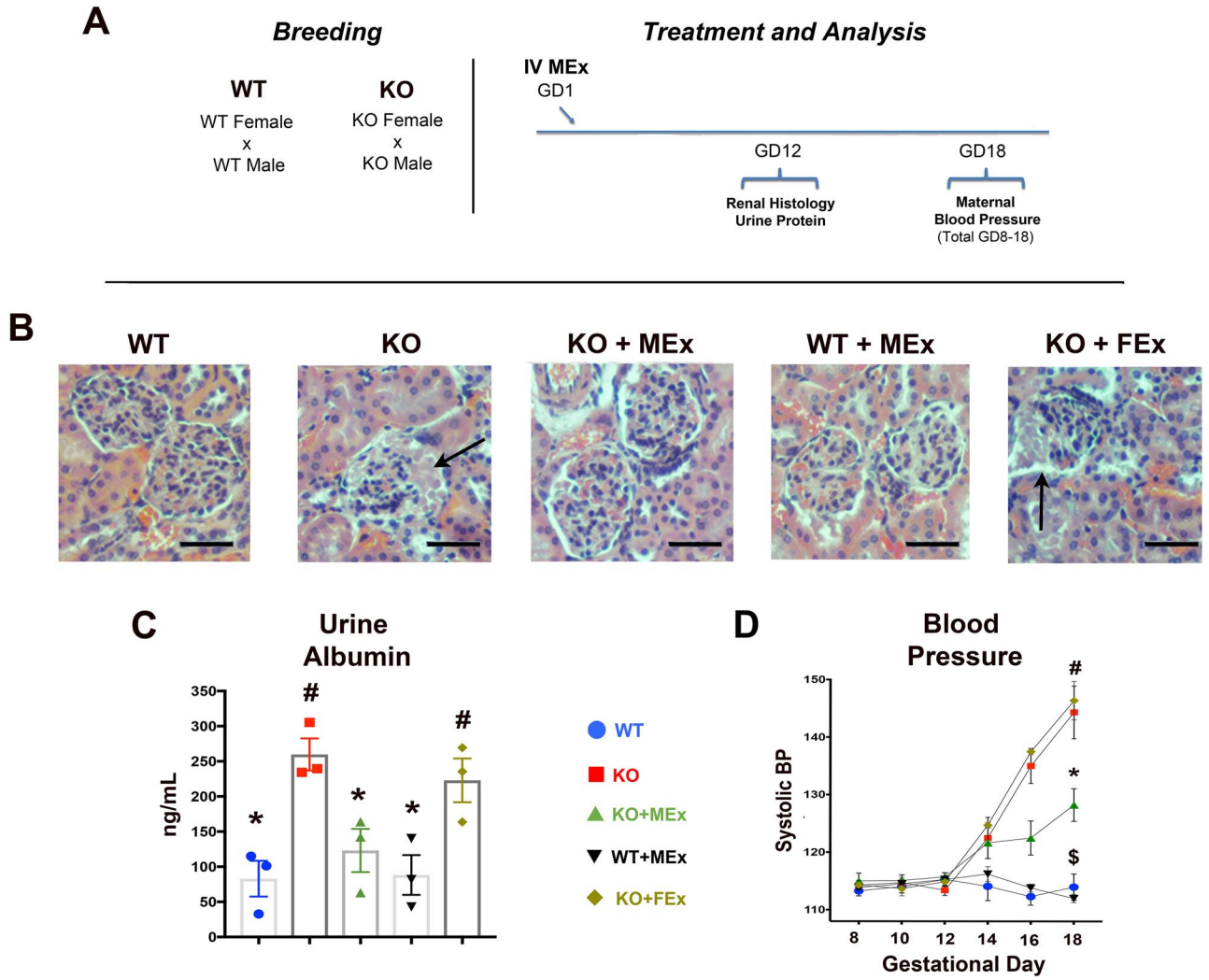

Figure 3. MEx therapy attenuates maternal renal pathology and hypertension. (A) Experimental design. (B) H&E histology of renal glomeruli at GD12, Images 100x magnification, scale bars 50um. Black arrows denote areas of eosin-positive proteinaceous material. (C) ELISA analysis of maternal urine albumin at GD12. (D) Maternal tail-cuff blood pressure throughout gestation. All images and graphical analyses representative of three independent experiments, three to four pregnant dams/experiment. Statistical significance ($P < 0.05$), as determined by one-way analysis of variance, denoted by different symbols (*,#,S).

Histology

Formalin-fixed placentas and kidneys were subsequently processed by paraffin embedding, sectioning, and hematoxylin/eosin (H&E) per standard procedures. Maternal spiral artery morphology within placental tissues was analyzed via serial ×10 images of metrial gland/placental interface (5/placenta), followed by measurement of artery vessel wall:lumen ratio using ImageJ (imagej.nih.gov). Renal tissue was surveyed via serial ×10 images of the renal cortex (5/kidney), followed by comparative analysis of glomerular characteristics between experimental groups. Immunohistochemistry was performed using a primary antibody against smooth muscle actin (Sigma Aldrich) at a dilution of 1:200 followed by secondary antibody incubation and 3-amino-9-ethylcarbazole (AEC) development (HistostainPlus IHC kit, Thermo Fisher).

Urine analysis

At time of sacrifice on GD12 (as described above), bladders were exposed and urine was aspirated via bladder puncture with a sterile 1 mL 30-G syringe. Urine samples were subsequently snap frozen and banked at −80°C for further analysis. Upon collection of full experimental cohort, urine samples were quick thawed and processed for mouse albumin enzyme-linked immunosorbent assay (ELISA) analysis per manufacturer's instructions (Abcam).

Blood pressure

Tail-cuff blood pressures were measured using a BP-2000 series II Blood Pressure Analysis System (Visitech) per manufacturer's instructions. Briefly, after a 5-min incubation period on a warming platform (37°C), a tail cuff and a pulse transmitter were placed on the tail. After an additional 5-min period of stabilization, serial tracings were obtained. After a week of training, tail-cuff systolic blood pressures were recorded every other day for timepoints GD8, 10, 12, 14, 16, 18. Systolic blood pressure values were averaged from five replicates of 10 serial measurements per mouse per day (total approximately 20 min/day).

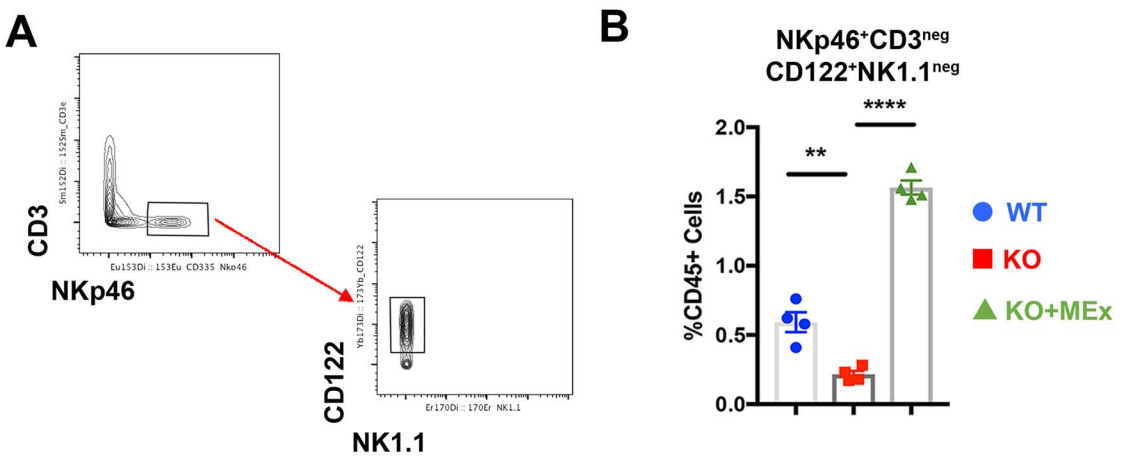

Figure 4. Uterine NK cells are restored by antenatal MEx administration. (A) Representative biaxial gating strategy for uNK cells. (B) Graphical analysis of uNK abundance changes between experimental groups. Data pooled from four independent experiments, three pregnant dams/experiment. Statistical significance as determined by one-way analysis of variance denoted as follows: $^{**}P < 0.01$, $^{****}P < 0.0001$. WT: wild-type pregnancy, KO: Hmox1$^{-/-}$ pregnancy, KO + MEx: Hmox$^{-/-}$ pregnancy treated with MEx.

Biodistribution of labeled extracellular vesicles (EV)

MSC-conditioned media from a total of 12 × 10^6 cells was harvested as described above followed by centrifugation at 100 000 × g for 1 h 10 min. Total EVs were then labeled with ExoGlow labeling kit per manufacturer's instructions (SystemBio). Labeled EVs were immediately injected into the tail vein of GD1 KO females (bred in homozygous matings). Following a 3-h incubation, uterine tissues were harvested and digested with collagenase Type IV and DNAse (Worthington). Tissue suspensions were treated with red blood cell (RBC) lysis buffer (Roche) and placed over a 40-µM cell strainer. The cell flow-through was pelleted, washed, and the resulting single-cell suspensions were spun onto charged microscope slides with a cytospin equipment. Slides were dried overnight, cover slipped with Fluorshield/DAPI solution (Invitrogen), and visualized using a Nikon Eclipse 80i microscope (Nikon, Tokyo, Japan).

Mass cytometry (CyTOF)

Six pooled IS tissues (fetus removed) from each pregnant dam were processed for mass cytometric analysis using the following method: IS were subjected enzymatic digestion with collagenase Type IV and DNAse (Worthington). Tissue suspensions were subsequently treated with RBC lysis buffer (Roche) and placed over a 40-µM cell strainer. The cell flow-through was pelleted, washed, and counted. Cells were stained with heavy metal-conjugated primary antibodies targeting a panel of 26 surface and intracellular markers (Supplemental Table S1), per manufacturer's protocol (Fluidigm), evaluating 0.8–1 × 10^6 cells per sample. Comparative *t*-distributed stochastic neighbor embedding (tSNE) analysis was performed using software standardized analysis parameters (Cytobank.org). Hierarchical cluster analysis was performed using FlowSOM analysis R-script software (Cytobank.org) with individual cluster threshold of 49. Further analysis of population frequency as well as mean metal intensity (MMI) of surface phenotype markers and cytokine expression were quantified using FlowJo software (Treestar).

Statistical analysis

GraphPad Prism software was used for all graphical and statistical analyses. One-way analysis of variance followed by a Tukey post hoc test for multiple comparisons was used in all statistical analyses between experimental groups. Differences were considered significant at $P < 0.05$. Throughout figures statistical significance was denoted by different symbols (*, #, $), or by number of asterisks (*) as follows: $^{*}P < 0.05$, $^{**}P < 0.01$, $^{***}P < 0.001$, $^{****}P < 0.0001$.

Study approval

All murine studies were approved by the Boston Children's Hospital Animal Care and Use Committee. All umbilical cord tissue collections were approved by the Boston Children's Hospital and Brigham and Women's Hospital Institutional Research Boards.

Results

Antenatal MEx therapy prevents pregnancy loss, fetal growth restriction, and preeclamptic physiology in Hmox1$^{-/-}$ mice

To explore the role of MEx treatment in the HO model, we bred Hmox1$^{-/-}$ (KO) or WT control females in homozygous mating pairs followed by evaluation of maternal and fetal parameters throughout pregnancy, four independent experiments, three to four pregnant dams per condition in each experiment. For treatment, a single dose of MEx (5 × 10^6 cell equivalents) was administered intravenously on GD1 to Hmox1$^{-/-}$ females (KO + MEx) (Figure 1A). This MEx dose was previously established in our lab as capable of conferring therapeutic effects in adult murine models of pulmonary hypertension and pulmonary fibrosis [12, 25]. At mid-pregnancy, KO pregnant females exhibited significant fetal loss as well as fetal growth restriction when compared with WT pregnancies, which was reversed with MEx treatment (Figure 1B–F). As a control, fibroblast-derived exosomes (FEx) were also tested and had no effect on fetal loss or fetal growth in KO mothers. Importantly, MEx did not alter fetal loss or growth parameters in WT pregnancies (Figure 1B–F).

A central hallmark of human preeclamptic physiology is lack of uterine spiral artery modification. In normal pregnancy, uterine arteries are transformed from small lumen vessels with a thick layer of outer smooth muscle into larger conduit thin-walled vessels by the end of the second trimester [2]. In preeclampsia, the remodeling of maternal spiral arteries is significantly reduced, characterized

by the sustained phenotype of small-lumen, thick-walled vessels, significantly impeding the oxygen and nutrient delivery to the fetus. In the placentas from KO pregnant females, we detected altered uterine artery remodeling within the utero-placental interface as compared with WT pregnancies, in both H&E and smooth muscle actin staining (Figure 2B–E). Interestingly, in KO females treated with MEx, uterine artery morphology was normalized, restoring the large-lumen, thin-walled phenotype seen in the WT pregnancies (Figure 2B–E). FEx had no effect on KO placental morphology and MEx did not alter placentas from WT pregnancies.

We further evaluated KO mothers for other stigmata of a preeclampsia-like phenotype. In evaluation of renal histology at GD12 from KO as compared with WT mothers, we identified areas of glomerular disruption and deposition of eosin-positive proteinaceous material in the KO maternal kidneys (Figure 3B), congruent with glomerular changes in Hmox1$^{+/-}$ pregnancies as well as other rodent preeclamptic models [22, 26]. We also identified a significant increase in proteinuria and systolic blood pressure in KO mothers (Figure 3B and C). Interestingly, glomerular pathology, proteinuria, and hypertension were all reversed following antenatal treatment with MEx (Figure 3B–D). Again, as control conditions, FEx had no effect on the renal and blood pressure parameters of KO pregnancies, and MEx did not alter these parameters in WT pregnancies.

In order to further evaluate the maternal contribution to the Hmox1$^{-/-}$ preeclampsia-like phenotype, we also conducted a series of hemizygous breedings comparing Hmox1$^{-/-}$ females × WT male matings with WT males × Hmox1$^{-/-}$ males: four independent experiments, three to four pregnant dams per condition in each experiment (Supplemental Figure S2A). These breedings resulted in all fetuses and placental tissues being Hmox1$^{+/-}$ with the experimental variable being the maternal genotype. Here, we also noted significant differences in fetal loss, fetal size, spiral artery changes, and glomerular morphology exclusively in breeding combinations with the maternal Hmox1$^{-/-}$ genotype, all of which were ameliorated by antenatal MEx therapy (Supplemental Figure S2B–H). These combined data demonstrate the capacity of antenatal MEx therapy to prevent maternal and fetal aspects of the Hmox1$^{-/-}$ preeclampsia-like phenotype.

Mass cytometric (CyTOF) analysis highlights multiple intrauterine immune modifications conferred by antenatal MEx therapy

In order to understand the means by which MEx alters the Hmox1$^{-/-}$ preeclamptic phenotype, we first investigated the biodistribution of MEx in KO females injected at treatment timepoint GD1. To accomplish this, we labeled EVs from MSC-conditioned media with a membrane-specific dye, ExoGlow. Three hours following injection, uterine tissues were harvested and enzymatically digested to form single-cell suspension followed by microscopic analysis of DAPI-stained cytospins (Supplemental Figure S3A). Evaluation of uterine tissues revealed a specific subset of cells positive for uptake of labeled EVs (Supplemental Figure S3B). Additional phenotypic labeling of cells was not possible due to technical limitations (fading) of the ExoGlow dye subsequent to further immunohistochemical analysis. Taken together, these data suggest that EVs injected in early pregnancy can be detected within cells of the preimplantation uterus.

As Hmox1 deficiency is known to be associated with alterations in immune regulation [18, 19], we next turned to investigation of the immune system at the maternal–fetal interface. Several studies, including our own work in pulmonary hypertension, pulmonary fibrosis, and experimental bronchopulmonary dysplasia have implicated immunomodulation as a primary mechanism by which MEx confer their therapeutic effects [7, 12, 25]. The immunological landscape of the maternal–fetal interface is comprised of several immune cell types with highly interconnected functions throughout pregnancy [27, 28]. Disruption of HO-1 in pregnancy has been associated with changes in natural killer (NK) cells, macrophages, and dendritic cells [22, 29, 30]. Given the interrelated assortment of leukocyte populations at play in the pathogenesis of preeclampsia [2], we chose to evaluate the impact of MEx therapy on the immunological landscape of the utero-placental interface in this model system by using multiparameter mass cytometry (CyTOF), which enables simultaneous analysis of several cell types within a tissue of interest [31].

At mid-pregnancy (GD12) we evaluated combined uterine, placenta, and metrial gland tissues (with fetus removed) using CyTOF analysis with a panel of 26 surface and intracellular markers (Supplemental Table S1). These tissues were taken from the same pregnancies as those evaluated for fetal loss, fetal size, and placental morphology (Figures 1 and 2): four independent experiments, three pregnant dams/experiment. While the immune populations of each of these tissues have been historically evaluated in separate analyses, our approach with combined tissues was to evaluate the global immune landscape at the utero-placental interface.

We first evaluated NK cell changes given their well-characterized role in preeclamptic pathogenesis as well as pregnancy loss [32]. Uterine NK (uNK) cells with a phenotype of NKp46^{+}CD122^{+}CD-3^{neg}NK1.1^{neg} [33] were significantly altered between experimental groups (Figure 4A and B). Previous studies have shown that uNK cells decrease in abundance in Hmox1$^{-/-}$ pregnancies [22], a trend which we also found in our uNK cell populations (Figure 4B). Interestingly, MEx therapy restored uNK cell abundance within IS to values similar to control pregnancies (Figure 4B).

We next screened for phenotypic shifts among experimental groups utilizing unbiased comparative tSNE plot analysis of all CD45^{+} cells. The most striking changes were noted in surface markers CD44, CD103, and CD64 (Figure 5, Supplemental Figure S4), which co-localized with myeloid lineage markers F4/80, CD11b, and CD11c (Figure 5). Relative abundance changes among all CD45^{+} cells were also evaluated using unsupervised FlowSOM hierarchical cluster analysis (Supplemental Figure S5). In this analysis, four clusters had significant abundance changes among experimental groups, all of which fell within myeloid lineages (Supplemental Figure S5, Supplemental Table S2).

Guided by these two unsupervised approaches, we then performed biaxial manual gating of all CD45^{+} cells, including myeloid subpopulations and their relative expression of CD44, CD103, and CD64 (Figure 6, Supplemental Figure S6). F4/80^{Hi}CD11b^{+} macrophages with both a CD11c^{Hi} and CD11c^{Lo} phenotype significantly increased in KO pregnancies and remained high in MEx-treated dams. Additionally, CD11c^{+}F4/80^{lo} cells distributed into CD11b hi/lo groups as has been previously shown for uterine cells with a dendritic cell phenotype [34]. While CD11b^{hi} cells were 10-fold more abundant overall, their percentages did not change significantly between all groups. CD11b^{lo} cells were elevated within KO pregnancies and remained high with MEx therapy. While CD44 was only significantly increased within F4/80^{Hi} macrophage populations in KO preeclamptic tissues, CD44 was consistently upregulated in all myeloid lineages in MEx-treated animals along

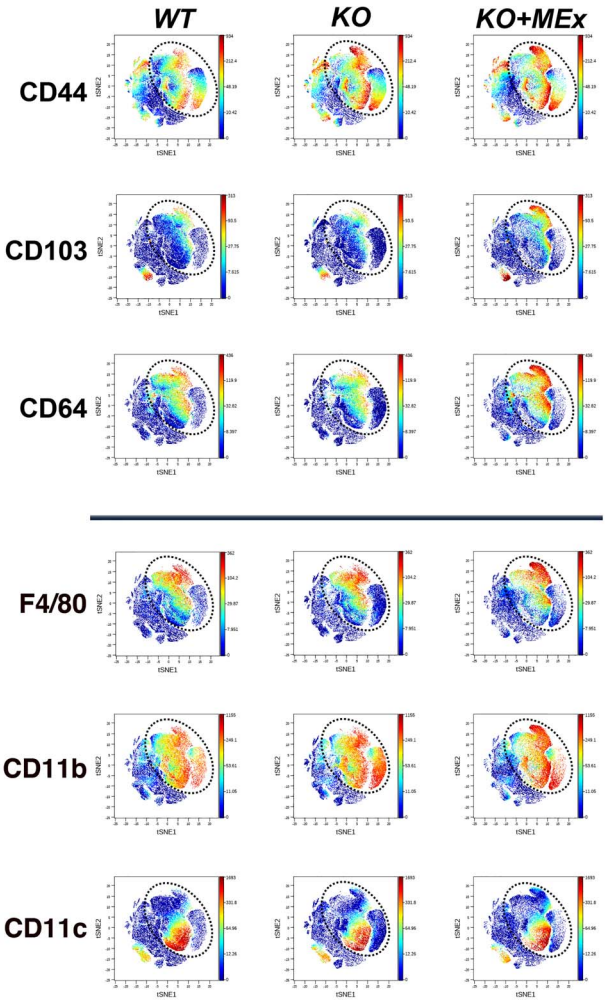

Figure 5. Antenatal MEx therapy confers phenotypic shifts among intrauterine myeloid populations. CyTOF analysis of GD12 utero-placental leukocytes. tSNE plots representative of four independent experiments, three pregnant dams/experiment. Dotted circle indicates area of prominent tSNE plot shifts between experimental groups. Multicolor scale indicates signal intensity for each surface marker.

with a dramatic increase in CD103 and CD64 (Figure 6). Of note, no other major leukocyte lineages showed significant changes in abundance between experimental groups (Supplemental Figure S6).

We next conducted a comparative analysis of intracellular cytokine expression among each of the major intrauterine immune cell lineages using MMI data from our CyTOF analysis (Figure 7) [35]. A targeted panel was analyzed, based on cytokines known to be significantly associated with both preeclampsia and pregnancy loss, namely interleukin-10 (IL-10), interferon-gamma (IFN-gamma), interleukin-6 (IL-6), and tumor necrosis factor-alpha (TNF-alpha) [2, 36–38]. Based on comparative analysis of MMI, we noted the intracellular cytokine repertoire to be globally changed in KO preeclamptic pregnancies and MEx treatment restored the profile similar to that of control WT pregnancies (Figure 7). Combined, these data show that preventative MEx treatment in the HO-1 null preeclampsia model significantly impacts multiple parameters of the intrauterine immune environment, resulting in key physiologic alterations that promote normalization of pregnancy and fetal growth.

Discussion

The results of this study demostrate that antenatal MEx therapy can signficiantly ameliorate preeclampsia-like physiology in the Hmox1 null preclinical model, preventing fetal loss and maternal symptoms with normalization of placental morphology and fetal growth. As the results of this study primarily capture a phenotype at mid-pregnancy (GD12), ongoing evaluations of embryo loss, fetal size, and placental morpohlogy throughout gestation in addition to postnatal growth will be key in ongoing characterization of the early and long-term effects of MEx treatment in Hmox1$^{-/-}$ pregnancies. In addition, as alterations in placental tissues of Hmox null pregnancies encompass a variety of changes in spiral artery morphology and junctional/labyrinth zones [21, 22], more detailed evaluation of trophoblast subpopulations will also be valuable for future studies of this model system. Given the sum consideration of our data, we propose that MEx treatment has significant therapeutic potential as a preventative modality for pregnancy loss, maternal preeclampsia-like physiology, and fetal growth restriction.

Utilizing biodistribution and multiparameter CyTOF immune analyses, we identified that systemically administered MEx can be visualized within the preimplantation uterus, and MEx treatment is associated with changes in multiple parameters of intrauterine leukocytes. In our study, all breeding combinations that resulted in a preeclampsia-like phenotype had the commonality of a maternal Hmox1 deficiency, with Hmox1$^{-/-}$ intrauterine maternal immune cells. The multiparameter changes highlighted by our CyTOF data suggest that alterations of the Hmox1$^{-/-}$ intrauterine immune phenotype may be a key avenue through which MEx confer their therapeutic benefit in these pregnancies. The most notable alterations were in uNK and myeloid cell abundance with significant increases of CD103 and CD64 expression within CD44^{hi} myeloid populations. Identifying alterations in uNK cells served as an important internal control, linking our study to previously published work demonstrating a significant decrease in uNK cells in the absence of Hmox1 [22]. In regard to myeloid phenotype changes, previous studies have identified CD44 upregulation as a marker of activation in both macrophage and dendritic cell phenotypes [39, 40]. Importantly, as these changes were observed at only mid-gestation, temporal evaluation of immunological alterations throughout gestation will be highly valuable to characterize the full scope of MEx immumodulatory effects in this model system.

CD103 is significantly associated with tolerance induction, particularly within populations of mucosal dendritic cells [41]. CD103 has also been identified on dendritic cell populations in the non-pregnant murine uterus distinguishing between CD11b low and high populations [34]. CD64 (the IgG receptor gamma chain) is a specific lineage identifier for murine intestinal macrophages and can be upregulated by increases in both IFN-gamma and IL-10 [42–44]. Whether CD64 upregulation is a reflection of the global cytokine shifts conferred by MEx therapy or the result of direct MEx modulation of myeloid populations warrants further investigation. Overall, our data suggest that CD103 and CD64 myeloid induction may be key components of immune homeostatic pathways to prevent preeclamptic onset.

Targeted analysis of cell-specific cytokine production also identified significant alterations in multiple cytokines associated with preeclamptic physiology and pregnancy loss. Among these findings, some key themes emerge. Specifically, IL-10 was reduced in all preeclamptic immune cell types and uniformly increased with MEx therapy. These findings are supported by previous studies showing

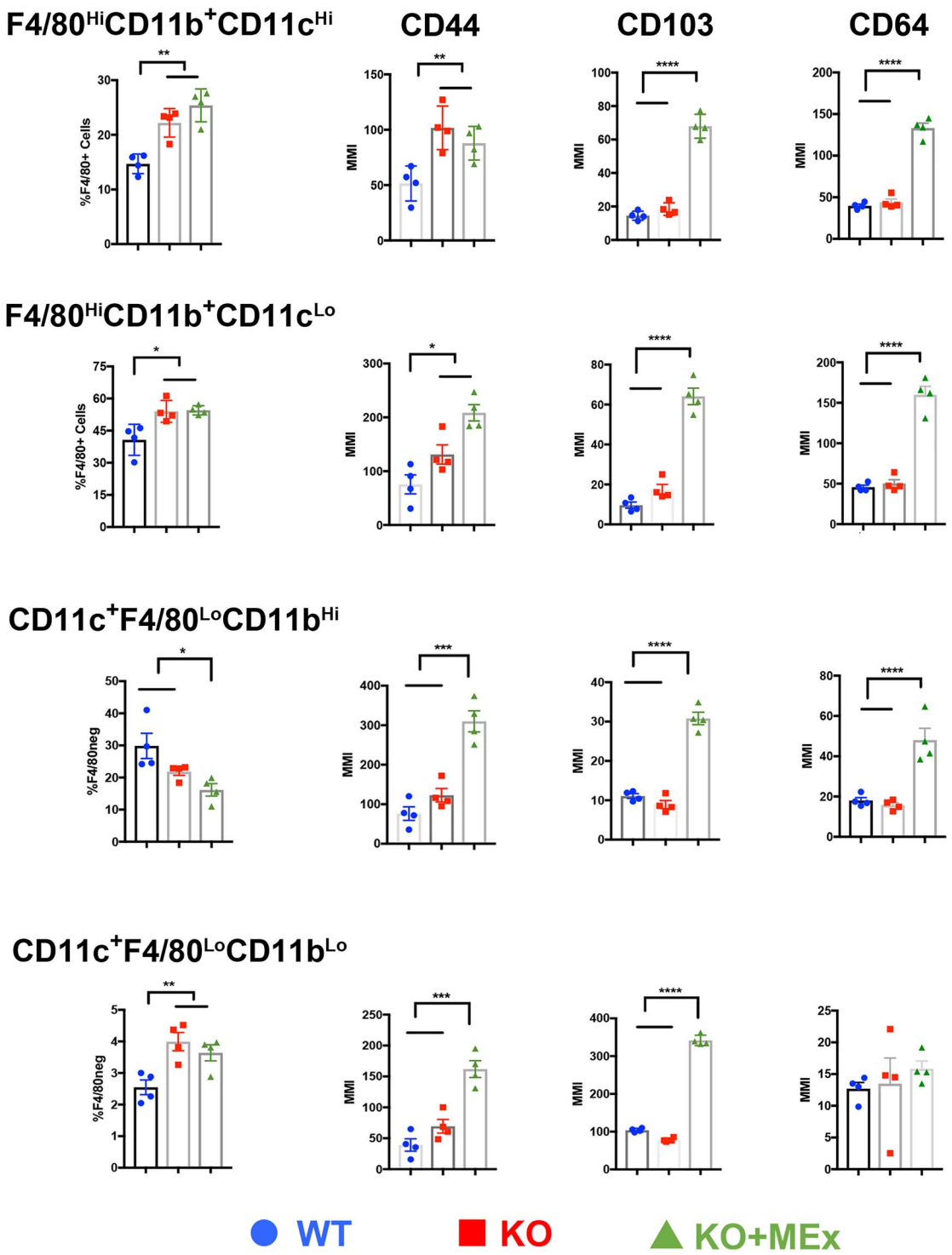

Figure 6. CD44, CD103, and CD64 are significantly upregulated in multiple myeloid subpopulations following MEx treatment. Graphical analysis from biaxial gating of myeloid population abundance and surface marker intensity from CyTOF evaluation of utero-placental leukocytes at GD12. Data pooled from four independent experiments, three pregnant dams/experiment. Statistical significance as determined by one-way analysis of variance is denoted as follows: $^{*}P < 0.05$, $^{**}P < 0.01$, $^{***}P < 0.001$, $^{****}P < 0.0001$.

decreased IL-10 expression in preeclamptic placentas [45, 46]. IFN-gamma, TNF-alpha, and IL-6 show different patterns of expression based on cell type. Up- or downregulation of these cytokines can have varying roles in normal pregnancy and disease states. For example, in early pregnancy, IFN-gamma is not only critical for the establishment of placentation [47], but is also persistently elevated in the serum of preeclamptic patients [38]. While additional cytokine evaluation is warranted, particularly in terms of correlating maternal serum cytokines with the intracellular cytokine content of intrauterine leukocytes, these data demonstrate the utility of using simultaneous,

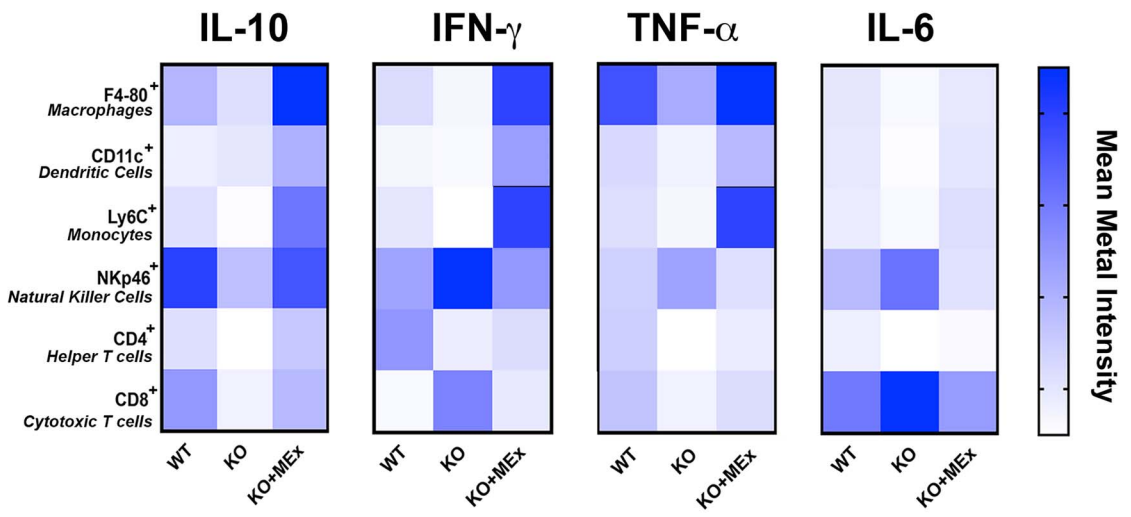

Figure 7. Multicellular cytokine profiles altered in preeclampsia are modulated by antenatal MEx therapy. Combined cytokine evaluation from relative MMI values from CyTOF intracellular cytokine analysis of utero-placental tissues at GD12. Data pooled from four independent experiments, three pregnant dams/experiment.

cell-specific analysis of cytokine changes. Our global comparative view of MEx-mediated immune changes in this model highlights contributions from macrophages, dendritic cells, and NK cells in the pathogenesis of a preeclampsia-like phenotype through a likely interrelated combination of cellular activation and cytokine secretion at the maternal–fetal interface. Further, as MEx were delivered systemically, evaluation of potential immunomodulatory effects on other maternal organ systems will also be interesting for future studies in this model system. These data highlight that therapeutics designed for preeclampsia need to address multiple parameters, rather than targeting isolated factors, likely a key reason why MEx therapy in this model was able to prevent multiple aspects of preeclampsia pathogenesis and sequelae.

The mechanisms by which MEx achieve intrauterine immunomodulation and prevention of preeclamptic physiology in this model system are likely multifactorial. As our MEx were prepared through a stringent isolation protocol targeted at minimizing co-isolation of non-EV material [7, 23], the effects of this therapy in our model system are likely via direct action of MEx on target cells. MEx contain a variety of key protein, lipid, and nucleic acid moieties that may work in synergy to confer their effects on target cell populations [23]. Further multiparameter analyses are needed to identify the pregnancy-specific molecular mechanisms through which MEx reprogram immune cells to promote prohomeostatic pathways and the congruent or hierarchical manner in which these immune changes confer uterine optimization to prevent preeclampsia. In conclusion, this study highlights the significant potential of maternally delivered MEx therapy to ameliorate preeclamptic physiology for the improvement of maternal and fetal health.

Supplementary material

Supplementary material is available at *BIOLRE* online.

Acknowledgments

Authors would like to acknowledge the Longwood Medical Area CyTOF Mass Cytometry Core for their contribution in the data acquisition and analysis of mass cytometry experiments.

Conflict of interest

SAM and SK are inventors of intellectual property technology licensed by Boston Children's Hospital to United Therapeutics Corporation.

Author Contributions

EST, AFG, and GRW participated in study design and execution, data collection, analysis, and manuscript writing; MR participated in study design and execution, analysis, and manuscript writing; VY participated in MEx preparation and characterization; XL participated in technical support; SAM and SK contributed to study design, supervision of study execution, analysis, manuscript writing, and final article editing and approval.

References

1. Mol BWJ, Roberts CT, Thangaratinam S, Magee LA, de Groot CJM, Hofmeyr GJ. Pre-eclampsia. *Lancet* 2016; **387**:999–1011.
2. Laresgoiti-Servitje E, Gomez-Lopez N, Olson DM. An immunological insight into the origins of pre-eclampsia. *Hum Reprod Update* 2010; **16**:510–524.
3. Deshmukh H, Way SS. Immunological basis for recurrent Fetal loss and pregnancy complications. *Annu Rev Pathol* 2019; **14**:185–210.
4. Germain AM, Romanik MC, Guerra I, Solari S, Reyes MS, Johnson RJ, Price K, Karumanchi SA, Valdes G. Endothelial dysfunction: a link among preeclampsia, recurrent pregnancy loss, and future cardiovascular events? *Hypertension* 2007; **49**:90–95.
5. Matthay MA, Anversa P, Bhattacharya J, Burnett BK, Chapman HA, Hare JM, Hei DJ, Hoffman AM, Kourembanas S, McKenna DH, Ortiz LA, Ott HC et al. Cell therapy for lung diseases. Report from an NIH-NHLBI workshop, November 13-14, 2012. *Am J Respir Crit Care Med* 2013; **188**:370–375.
6. Prockop DJ. The exciting prospects of new therapies with mesenchymal stromal cells. *Cytotherapy* 2017; **19**:1–8.
7. Willis GR, Fernandez-Gonzalez A, Anastas J, Vitali SH, Liu X, Ericsson M, Kwong A, Mitsialis SA, Kourembanas S. Mesenchymal stromal cell exosomes ameliorate experimental bronchopulmonary dysplasia and restore lung function through macrophage immunomodulation. *Am J Respir Crit Care Med* 2018; **197**:104–116.

8. Hansmann G, Fernandez-Gonzalez A, Aslam M, Vitali SH, Martin T, Mitsialis SA, Kourembanas S. Mesenchymal stem cell-mediated reversal of bronchopulmonary dysplasia and associated pulmonary hypertension. *Pulm Circ* 2012; **2**:170–181.
9. Phinney DG, Pittenger MF. Concise review: MSC-derived exosomes for cell-free therapy. *Stem Cells* 2017; **35**:851–858.
10. Aslam M, Baveja R, Liang OD, Fernandez-Gonzalez A, Lee C, Mitsialis SA, Kourembanas S. Bone marrow stromal cells attenuate lung injury in a murine model of neonatal chronic lung disease. *Am J Respir Crit Care Med* 2009; **180**:1122–1130.
11. van Haaften T, Byrne R, Bonnet S, Rochefort GY, Akabutu J, Bouchentouf M, Rey-Parra GJ, Galipeau J, Haromy A, Eaton F, Chen M, Hashimoto K et al. Airway delivery of mesenchymal stem cells prevents arrested alveolar growth in neonatal lung injury in rats. *Am J Respir Crit Care Med* 2009; **180**:1131–1142.
12. Lee C, Mitsialis SA, Aslam M, Vitali SH, Vergadi E, Konstantinou G, Sdrimas K, Fernandez-Gonzalez A, Kourembanas S. Exosomes mediate the cytoprotective action of mesenchymal stromal cells on hypoxia-induced pulmonary hypertension. *Circulation* 2012; **126**:2601–2611.
13. Sdrimas K, Kourembanas S. MSC microvesicles for the treatment of lung disease: a new paradigm for cell-free therapy. *Antioxid Redox Signal* 2014; **21**:1905–1915.
14. Colombo M, Raposo G, Thery C. Biogenesis, secretion, and intercellular interactions of exosomes and other extracellular vesicles. *Annu Rev Cell Dev Biol* 2014; **30**:255–289.
15. Mitsialis SA, Kourembanas S. Stem cell-based therapies for the newborn lung and brain: possibilities and challenges. *Semin Perinatol* 2016; **40**:138–151.
16. Grimes S, Bombay K, Lanes A, Walker M, Corsi DJ. Potential biological therapies for severe preeclampsia: A systematic review and meta-analysis. *BMC Pregnancy Childbirth* 2019; **19**:163.
17. Suvakov S, Richards C, Nikolic V, Simic T, McGrath K, Krasnodembskaya A, McClements L. Emerging therapeutic potential of mesenchymal stem/stromal cells in preeclampsia. *Curr Hypertens Rep* 2020; **22**:37.
18. Ozen M, Zhao H, Lewis DB, Wong RJ, Stevenson DK. Heme oxygenase and the immune system in normal and pathological pregnancies. *Front Pharmacol* 2015; **6**:84.
19. Naito Y, Takagi T, Higashimura Y. Heme oxygenase-1 and anti-inflammatory M2 macrophages. *Arch Biochem Biophys* 2014; **564**:83–88.
20. Meyer N, Langwisch S, Scharm M, Zenclussen AC. Using ultrasound to define the time point of intrauterine growth retardation in a mouse model of heme oxygenase-1 deficiency. *Biol Reprod* 2020 (in press). Published online ahead of print 28 April 2020. doi: 10.1093/biolre/ioaa057.
21. Peoc'h K, Puy V, Fournier T. Haem oxygenases play a pivotal role in placental physiology and pathology. *Hum Reprod Update* 2020 (in press). Published online ahead of print 29 April 2020. doi: 10.1093/humupd/dmaa014.
22. Zenclussen ML, Linzke N, Schumacher A, Fest S, Meyer N, Casalis PA, Zenclussen AC. Heme oxygenase-1 is critically involved in placentation, spiral artery remodeling, and blood pressure regulation during murine pregnancy. *Front Pharmacol* 2014; **5**:291.
23. Willis GR, Kourembanas S, Mitsialis SA. Toward exosome-based therapeutics: isolation, heterogeneity, and fit-for-purpose potency. *Front Cardiovasc Med* 2017; **4**:63.
24. Yet SF, Perrella MA, Layne MD, Hsieh CM, Maemura K, Kobzik L, Wiesel P, Christou H, Kourembanas S, Lee ME. Hypoxia induces severe right ventricular dilatation and infarction in heme oxygenase-1 null mice. *J Clin Invest* 1999; **103**:R23–R29.
25. Mansouri N, Willis GR, Fernandez-Gonzalez A, Reis M, Nassiri S, Mitsialis SA, Kourembanas S. Mesenchymal stromal cell exosomes prevent and revert experimental pulmonary fibrosis through modulation of monocyte phenotypes. *JCI Insight* 2019; **4**:e128060.
26. Li Z, Zhang Y, Ying Ma J, Kapoun AM, Shao Q, Kerr I, Lam A, O'Young G, Sannajust F, Stathis P, Schreiner G, Karumanchi SA et al. Recombinant vascular endothelial growth factor 121 attenuates hypertension and improves kidney damage in a rat model of preeclampsia. *Hypertension* 2007; **50**:686–692.
27. Petroff MG. Immune interactions at the maternal-fetal interface. *J Reprod Immunol* 2005; **68**:1–13.
28. Taglauer ES, Adams Waldorf KM, Petroff MG. The hidden maternal-fetal interface: events involving the lymphoid organs in maternal-fetal tolerance. *Int J Dev Biol* 2010; **54**:421–430.
29. Schumacher A, Wafula PO, Teles A, El-Mousleh T, Linzke N, Zenclussen ML, Langwisch S, Heinze K, Wollenberg I, Casalis PA, Volk HD, Fest S et al. Blockage of heme oxygenase-1 abrogates the protective effect of regulatory T cells on murine pregnancy and promotes the maturation of dendritic cells. *PLoS One* 2012; **7**:e42301.
30. Zhao H, Kalish F, Wong RJ, Stevenson DK. Infiltration of myeloid cells in the pregnant uterus is affected by heme oxygenase-1. *J Leukoc Biol* 2017; **101**:217–226.
31. Kimball AK, Oko LM, Bullock BL, Nemenoff RA, van Dyk LF, Clambey ETA. Beginner's guide to Analyzing and visualizing mass cytometry data. *J Immunol* 2018; **200**:3–22.
32. Hatta K, MacLeod RJ, Gerber SA, Croy BA. Emerging themes in uterine natural killer cell heterogeneity and function. *Am J Reprod Immunol* 2012; **68**:282–289.
33. Yadi H, Burke S, Madeja Z, Hemberger M, Moffett A, Colucci F. Unique receptor repertoire in mouse uterine NK cells. *J Immunol* 2008; **181**:6140–6147.
34. Collins MK, Tay CS, Erlebacher A. Dendritic cell entrapment within the pregnant uterus inhibits immune surveillance of the maternal/fetal interface in mice. *J Clin Invest* 2009; **119**:2062–2073.
35. Erlebacher A. Immunology of the maternal-fetal interface. *Annu Rev Immunol* 2013; **31**:387–411.
36. Robertson SA, Chin PY, Femia JG, Brown HM. Embryotoxic cytokines-potential roles in embryo loss and fetal programming. *J Reprod Immunol* 2018; **125**:80–88.
37. Lash GE, Ernerudh J. Decidual cytokines and pregnancy complications: focus on spontaneous miscarriage. *J Reprod Immunol* 2015; **108**:83–89.
38. Szarka A, Rigo J Jr, Lazar L, Beko G, Molvarec A. Circulating cytokines, chemokines and adhesion molecules in normal pregnancy and preeclampsia determined by multiplex suspension array. *BMC Immunol* 2010; **11**:59.
39. Qadri M, Almadani S, Jay GD, Elsaid KA. Role of CD44 in regulating TLR2 activation of human macrophages and downstream expression of proinflammatory cytokines. *J Immunol* 2018; **200**:758–767.
40. Nedvetzki S, Sowinski S, Eagle RA, Harris J, Vely F, Pende D, Trowsdale J, Vivier E, Gordon S, Davis DM. Reciprocal regulation of human natural killer cells and macrophages associated with distinct immune synapses. *Blood* 2007; **109**:3776–3785.
41. Scott CL, Aumeunier AM, Mowat AM. Intestinal CD103+ dendritic cells: master regulators of tolerance? *Trends Immunol* 2011; **32**:412–419.
42. Fanger NA, Voigtlaender D, Liu C, Swink S, Wardwell K, Fisher J, Graziano RF, Pfefferkorn LC, Guyre PM. Characterization of expression, cytokine regulation, and effector function of the high affinity IgG receptor fc gamma RI (CD64) expressed on human blood dendritic cells. *J Immunol* 1997; **158**:3090–3098.
43. Cassatella MA, Flynn RM, Amezaga MA, Bazzoni F, Vicentini F, Trinchieri G. Interferon gamma induces in human neutrophils and macrophages expression of the mRNA for the high affinity receptor for monomeric IgG (fc gamma R-I or CD64). *Biochem Biophys Res Commun* 1990; **170**:582–588.
44. Bovolenta C, Gasperini S, McDonald PP, Cassatella MA. High affinity receptor for IgG (fc gamma RI/CD64) gene and STAT protein binding to the IFN-gamma response region (GRR) are regulated differentially in human neutrophils and monocytes by IL-10. *J Immunol* 1998; **160**:911–919.
45. Hennessy A, Pilmore HL, Simmons LA, Painter DM. A deficiency of placental IL-10 in preeclampsia. *J Immunol* 1999; **163**:3491–3495.
46. Makris A, Xu B, Yu B, Thornton C, Hennessy A. Placental deficiency of interleukin-10 (IL-10) in preeclampsia and its relationship to an IL10 promoter polymorphism. *Placenta* 2006; **27**:445–451.
47. Murphy SP, Tayade C, Ashkar AA, Hatta K, Zhang J, Croy BA. Interferon gamma in successful pregnancies. *Biol Reprod* 2009; **80**:848–859.